JOURNAL OF MATERIALS SCIENCE 31 (1996) 1375–1388

Microstructure, tensile properties and fracture behaviour of Al_2O_3 particulate-reinforced aluminium alloy metal matrix composites

T. S. SRIVATSAN
Department of Mechanical Engineering, The University of Akron, Akron, OH 44325-3903, USA

The tensile deformation and fracture behaviour of aluminium alloy 2014 discontinuously-reinforced with particulates of Al_2O_3 was studied with the primary objective of understanding the influence of reinforcement content on composite microstructure, tensile properties and quasi-static fracture behaviour. Results reveal that elastic modulus and strength of the metal-matrix composite increased with reinforcement content in the metal matrix. With increase in test temperature the elastic modulus showed a marginal decrease while the ductility exhibited significant improvement. The improved strength of the Al–Al_2O_3 composite is ascribed to the concurrent and mutually interactive influences of residual stresses generated due to intrinsic differences in thermal expansion coefficients between constituents of the composite, constrained plastic flow and triaxiality in the soft and ductile aluminium alloy matrix due to the presence of hard and brittle particulate reinforcements. Fracture on a microscopic scale initiated by cracking of the individual or agglomerates of Al_2O_3 particulates in the metal matrix and decohesion at the matrix–particle interfaces. Failure through cracking and decohesion at the interfaces increased with reinforcement content in the matrix. The kinetics of the fracture process is discussed in terms of applied far-field stress and intrinsic composite microstructural effects.

1. Introduction

The need for lightweight and high performance structural materials to satisfy the demands of the aerospace, automotive and consumer-related industries provided the necessary impetus for the development and emergence of metal-matrix composites (MMCs) as attractive and viable alternatives to the traditional engineering alloys. A large majority of these composite materials are metallic matrices reinforced with high strength, high modulus and brittle ceramic phases which can be either continuous in the form of fibre or discontinuous in the form of whisker, platelet and particulate reinforcements embedded in a ductile metallic matrix. The reinforced metal matrices offer potential for improvements in efficiency, mechanical performance and reliability over the newer generation monolithic alloys.

Ceramic fibre-reinforced MMCs offer a spectrum of advantages in applications where high strength and high stiffness are of primary concern. Although the continuous fibre-reinforced metal matrices offer highly directional properties such as high specific stiffness along the reinforcement direction [1], the discontinuously-reinforced metal matrices based on whiskers, particulates or nodules as the reinforcing phase are preferred since they offer a number of advantages. In particular, incorporation of discontinuous ceramic reinforcements in an aluminium alloy metal matrix offers improvements in elastic modulus, wear resistance, strength, structural efficiency, reliability and control of physical properties such as density and coefficient of thermal expansion, thereby, providing improved mechanical performance in comparison to the unreinforced metal matrix [2–11]. In fact, the discontinuous ceramic particulate reinforced aluminium alloy metal matrix offers advantages such as a 15–40% increase in strength and a 30–50% increase in stiffness [12, 13], low density, while generally maintaining receptiveness to processing and characterization techniques used for the conventional unreinforced counterparts. An increase in modulus of greater than 100 per cent have been reported for aluminium alloys reinforced with a volume fraction of 40% silicon carbide particulates (SiC_p) [14]. From a design perspective the attractiveness stems from an improvement in specific modulus, i.e. density-compensated increase in elastic modulus. Besides, the discontinuously reinforced MMCs provide the additional advantage of being machinable and workable.

The ceramic particle reinforced aluminium alloy metal matrices can be synthesized by ingot metallurgy, powder metallurgy and mechanical alloying processing techniques. Each of these processing techniques results in a composite having different properties. The aluminium alloy MMCs based on particulate reinforcements are particularly attractive because they can

0022–2461

be made with properties that are isotropic in three dimensions or in two dimension. Furthermore, conventional aluminium alloy fabrication methods can be used to deform the ingot or billet to produce a wide range of product forms. However, the primary disadvantages with the ceramic particle-reinforced matrices is that they suffer from low strain-to-failure, inadequate fracture toughness and inferior fatigue crack growth and fracture resistance compared to that of the unreinforced matrix material [15–25].

The present study was undertaken with the objective of evaluating the influence of ceramic particulate reinforcements on the microstructure, tensile properties and fracture behaviour of an aluminium alloy MMC. In the experimental programme the tensile properties and fracture behaviour were evaluated for two different volume fractions of the ceramic particle reinforcement in the aluminium alloy matrix, at ambient and elevated temperatures. The ambient temperature properties are compared with those at the elevated temperature in order to rationalize temperature influences on tensile deformation and fracture behaviour.

2. Material

The composite material (MMC) selected for investigation in this study was based on aluminium alloy 2014 discontinuously reinforced with varying volume fractions of Al_2O_3 particulates. The aluminium alloy MMCs were made using a proprietory casting technique by DURAL Aluminium Composites Corporation (DURALCAN USA, San Diego, CA). Two different volume fractions (10 and 15 vol %) of the discontinuous particulate Al_2O_3 phase were chosen. The nominal chemical composition (in weight percent) of the matrix alloy is given in Table I. The iron and silicon elements in the alloy are impurities. The ingot metallurgy-based Al_2O_3 particulate-reinforced 2014 composite was provided as an extruded billet. The billet was obtained by extruding the cast ingot at 450 °C through a standard shear-face die. The starting ingot was 178 mm and was extruded with an extrusion ratio of 17:1 to produce rectangular blanks of size 19 mm × 76 mm. The extruded material was solutionized at 502 °C for 2 h, cold water quenched, and artificially aged at 160 °C for 2 h to get the peak-aged (T6) condition. The 2014/Al_2O_3/xxp MMCs were provided by DURALCAN USA.

3. Experimental techniques

3.1. Microstructural evaluation

Metallographic samples were cut from the as-received 2014/Al_2O_3/xxp composites, mounted in bakelite and wet ground on 320, 400 and 600 grit silicon carbide (SiC) paper using water as lubricant and then mechanically polished with one micron alumina-based polishing compound. Particle morphology, their size and distribution in the aluminium alloy metal matrix, and other intrinsic microstructural features were examined in an optical microscope and photographed using the standard bright-field technique.

TABLE I Chemical composition of matrix Al–Cu–Mg alloy 2014 (wt %)

Element	Cu	Mg	Mn	Si	Al
(wt %)	4.4	0.5	0.8	0.8	Balance

Tensile test specimens were precision machined from blanks of size 150 mm × 20 mm × 20 mm using a diamond coated saw blade. The specimens were machined with the stress axis parallel to the extrusion direction and conformed to standards specified in ASTM: E-8. The test specimens were smooth and cylindrical in the gauge section which measured 6.25 mm in diameter and 25 mm in length. To minimize the effects of surface irregularities and finish, final surface preparation was achieved by mechanically polishing the entire gauge section of the test specimens through 600 grit silicon carbide paper to remove all circumferential scratches and surface machine marks.

Uniaxial tensile tests were performed on a fully automated, computer controlled servohydraulic test machine equipped with a 10 000 kg load cell. The load train was aligned prior to the initiation of testing to minimize specimen bending. The tests were performed at room temperature (27 °C) and elevated temperatures of 100 and 180 °C. The elevated temperature tests were performed using an INSTRON Environmental Chamber System (Model 3111) unit. The temperature was controlled with the aid of a temperature controller linked to a thermocouple fixed to the specimen's surface. The maximum temperature variation along the gauge length was ±2 °C. The composite specimens were deformed at a constant strain rate of 0.0001 s^{-1}. The stress and strain parallel to the load line was recorded on an X–Y recorder equipped with a pen plotter.

Fracture surfaces of the deformed tensile specimens were comprehensively examined in a scanning electron microscope (SEM) to characterize the predominant fracture mode and the fine-scale features on the tensile fracture surface. Samples for SEM observation were obtained from the deformed tensile specimens by sectioning parallel to the fracture surface.

4. Results and discussion

4.1. Initial microstructure

The triplanar optical micrographs illustrating the microstructure of the 2014/Al_2O_3/xxp composites, for two volume fractions of the discontinuous particulate reinforcement phase, are shown in Figs 1 and 2. The Al_2O_3 particulates, in the composite matrix, were non-uniform in size, irregularly shaped and dispersed randomly through the metal matrix. Few of the particles had sharp corners. At regular intervals clustering or agglomeration of the Al_2O_3 particulates, of varying size, was observed resulting in particulate-rich and particulate-depleted regions. An agglomerated site consisted of the smaller particles of varying sizes and shapes intermingled with a few larger particles which appeared either rectangular or oblong in shape. The degree of agglomeration or clustering of the Al_2O_3

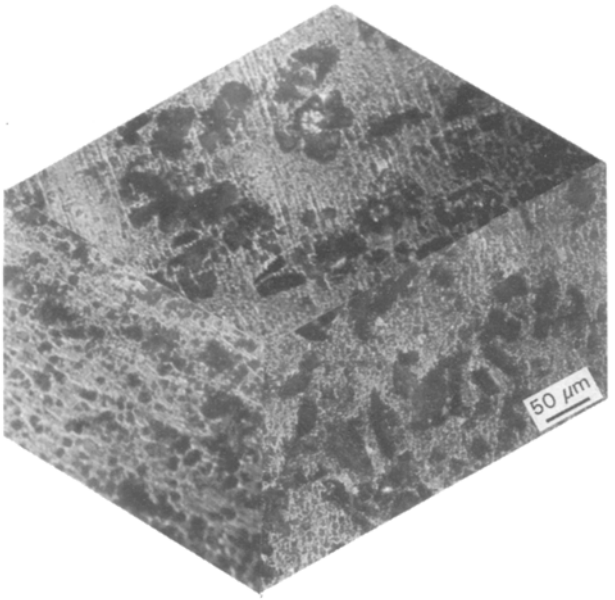

Figure 1 Triplanar optical micrograph illustrating microstructure of the 2014/Al_2O_3/10p composite.

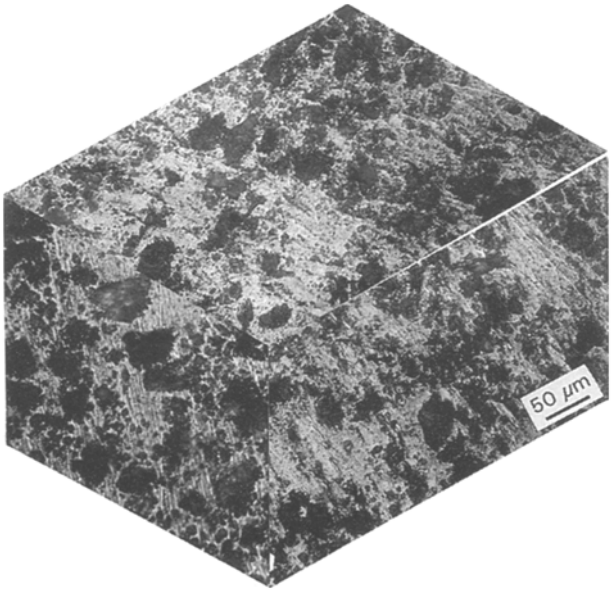

Figure 2 Triplanar optical micrograph illustrating microstructure of the 2014/Al_2O_3/15p composite.

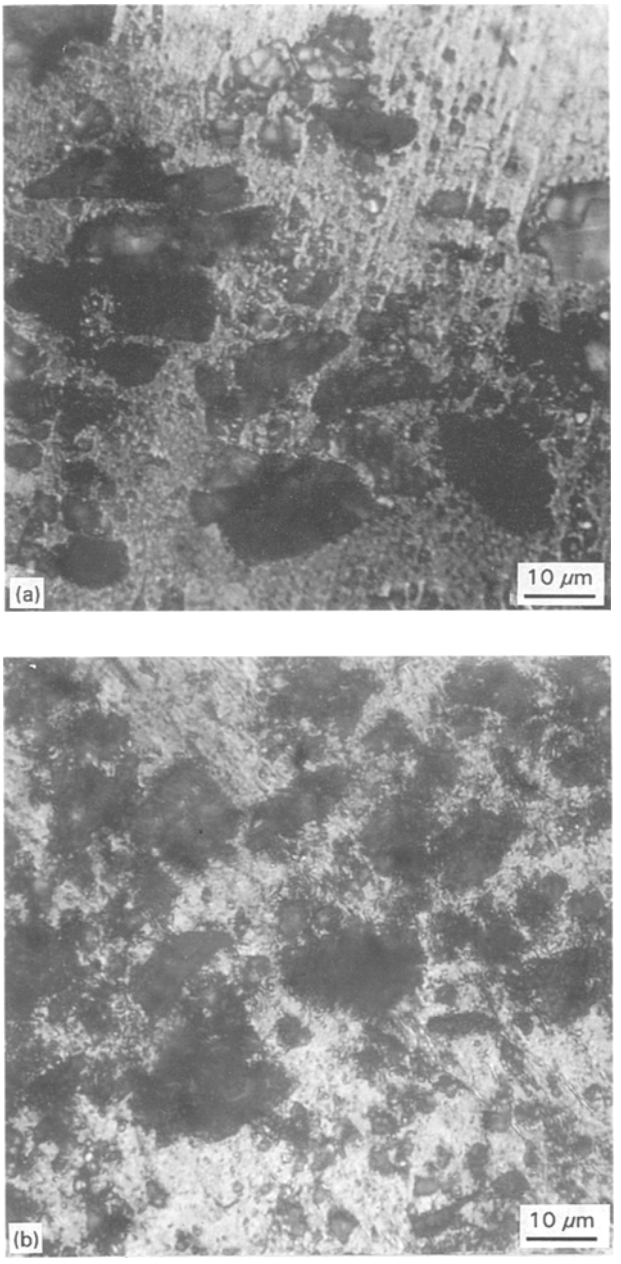

Figure 3 Optical micrograph showing clustering or agglomeration of the Al_2O_3 particles: (a) 2014/Al_2O_3/10p, and (b) 2014/Al_2O_3/15p

particulates was found to increase with an increase in the amount of reinforcement phase in the 2014 aluminium alloy metal matrix (Fig. 3). The non-uniform distribution of the Al_2O_3 particulates along the three orthogonal directions (extrusion, long transverse and short transverse) results in an anisotropic microstructure of the 2014/Al_2O_3/xxp composites. No attempt was made in this study to determine the particle size distribution for the two composite materials.

4.2. Tensile properties

The tensile properties of the 2014/Al_2O_3/xxp MMCs, for the two different volume fractions of ceramic particle (Al_2O_3) reinforcement, at ambient (27 °C) and elevated temperatures (100 and 180 °C), are summarized in Table II.

4.2.1. Elastic modulus

Tensile test results reveal an increase in elastic modulus with an increase in Al_2O_3 content in the aluminium alloy metal matrix, at both ambient temperature (27 °C) and elevated temperature (100 °C). However, at the elevated temperature of 180 °C the elastic modulus of the 2014/Al_2O_3/15p composite is marginally lower than that of the 2014/Al_2O_3/10p counterpart. The effect of reinforcement content and test temperature on modulus of the composites is shown in Fig. 4. At room temperature (27 °C) the elastic modulus of the 2014 alloy with 15 vol % Al_2O_3 is 101 GPa, which is:

(a) 45 per cent more than the elastic modulus of the matrix alloy with no reinforcement (71 GPa), that is,

TABLE II Monotonic properties of 2014/Al_2O_3 metal-matrix composites

Reinforcement (f_v) (%)	Temperature (°C)	Young's Modulus (E) (Gpa)	(10^3 Ksi)	Yield stress (σ_y) (Mpa)	(Ksi)	Ultimate tensile strength (σ_{UTS}) (Mpa)	(Ksi)	Fracture stress (σ_f) (Mpa)	(Ksi)	ε_f (%)	RA (%)	$\ln\left(\frac{A_o}{A_f}\right)$ (%)
10	24[a]	92	(13)	460	(64)	495	(69)	490	(68)	2.0	6.30	6.5
	100	84	(12)	416	(58)	434	(61)	400	(56)	5.2	9.34	9.8
	180	83	(11.6)	325	(45)	340	(47)	255	(36)	6.6	11.60	12.4
15	24[a]	101	(14)	470	(65)	510	(71)	495	(69)	2.7	4.70	4.9
	100	89	(12)	420	(59)	445	(62)	400	(56)	5.6	7.84	8.2
	180	79	(11)	310	(44)	325	(45)	240	(34)	6.2	10.10	10.7

[a] Result based on average of two tests.
ε_f – Strain to failure.
f_v – Volume fraction (%) reinforcement.
RA – Reduction in area.
$\ln\left(\frac{A_o}{A_f}\right)$ – Tensile ductility.

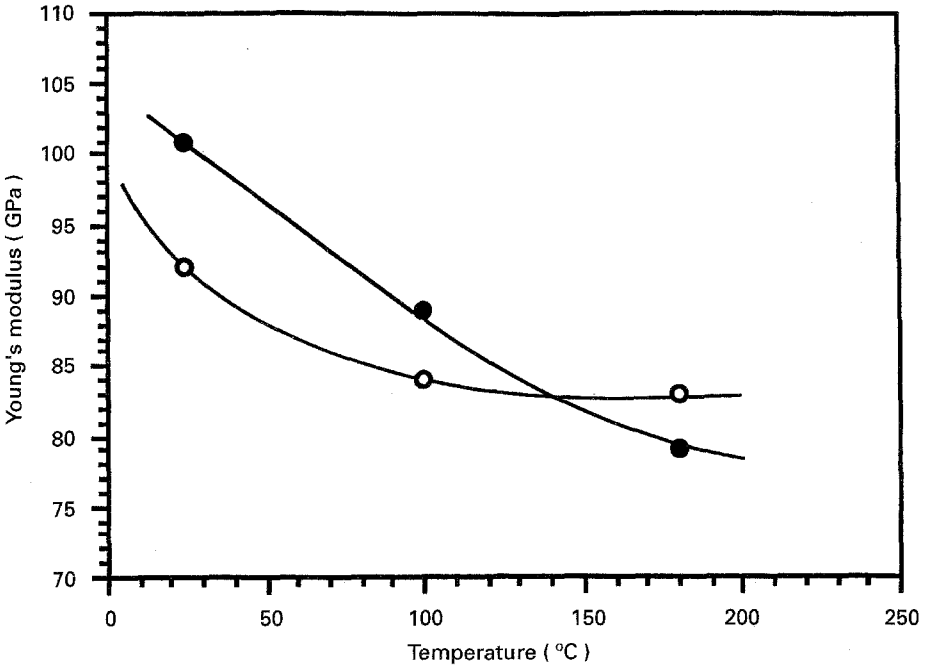

Figure 4 Effect of test temperature and reinforcement content on elastic modulus of 2014/Al_2O_3 composites. Key: (○) 10% Al_2O_3; (●) 15% Al_2O_3.

the unreinforced metal matrix (aluminium alloy 2014), and

(b) 10 per cent more than the elastic modulus of the 2014 matrix with 10 vol % of Al_2O_3 (92 GPa).

Furthermore, for both volume fractions of the discontinuous Al_2O_3 reinforcement phase in the metal matrix, the elastic modulus decreased with an increase in test temperature. The degradation was as high as 10 per cent for the 2014/Al_2O_3/10p composite and 20 per cent for the 2014/Al_2O_3/20p composite counterpart.

4.2.2. Strength

The yield strength, defined as the stress corresponding to a plastic strain of 0.2%, increased with an increase in the Al_2O_3 particulate reinforcement phase in the 2014 aluminium alloy metal matrix. The observed increase was however only marginal.

(a) At ambient temperature the 2014/Al_2O_3/15p composite had only a two per cent higher yield strength (470 MPa) than the 2014/Al_2O_3/10p composite counterpart (460 MPa).

(b) At 100 °C, the improvement or increase in yield strength of the 2014/Al_2O_3/ 15p composite over the 2014/Al_2O_3/10p counterpart is only marginal (one per cent).

(c) At 180 °C, the composite with higher volume fraction of the discontinuous Al_2O_3 reinforcement (15 vol %) had lower yield strength than the composite with lower volume fraction of the discontinuous

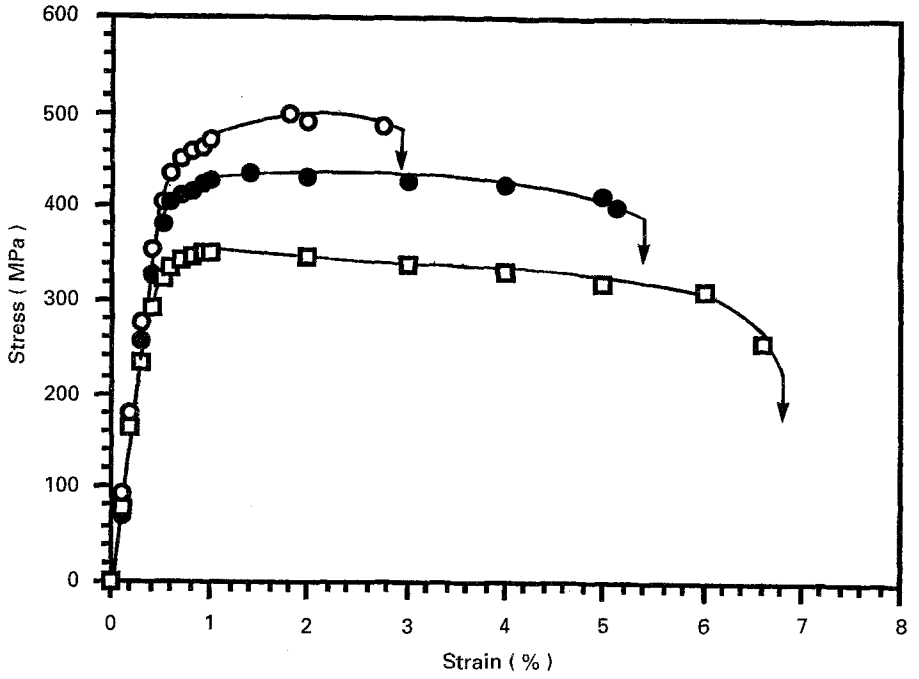

Figure 5 Effect of test temperature on engineering stress engineering strain curves of the 2014/Al_2O_3/10p composite. Key: (○) 25 °C; (●) 100 °C; (□) 180 °C.

reinforcement (10 vol %). An observation consistent with the lower modulus of this composite at this temperature.

The ultimate tensile strength of the composite is marginally more than the tensile yield strength indicating that the work hardening rate past yielding is low. The ultimate tensile strength followed the same trend as the yield strength of the composite. The improvement in strength of the 2014/Al_2O_3/15p composite over the 2014/Al_2O_3/10p composite counterpart was only marginal at the lower test temperatures (27 and 100 °C) and decreased at the higher test temperature of 180 °C.

Whereas, the yield strength and ultimate tensile strength of the 2014/Al_2O_3 composites are only marginally influenced by competing and mutually interactive influences of Al_2O_3 particulate reinforcement phase in the ductile 2014 matrix and test temperature, the ductility as measured by: (i) tensile elongation over 12.7 mm gauge length of the test specimen, and (ii) reduction in cross-sectional area, decreases with an increase in the Al_2O_3 particle reinforcement phase in the 2014 metal matrix. This observation is consistent with the strength improvement, though marginal, achieved with increased Al_2O_3 particulate reinforcement phase in the 2014 matrix. However, for both volume fractions of the Al_2O_3 particulate reinforcement phase, the reduction in area and tensile ductility increases with an increase in test temperature. The strain-to-failure (ε_f) of the 2014/Al_2O_3/xxp MMCs increases with an increase in test temperature, and is consistent with the degradation of both strength and stiffness at the higher test temperatures. A comparison of the stress–strain curves, of each MMC, at the three test temperatures, is made in Figs 5 and 6. Variation of strength with test temperature is exemplified in Fig. 7.

The manner in which reinforcement particle size and volume fraction affects ultimate tensile strength can be best described in terms of work hardening. Beyond macroscopic yield the stress–strain curve is well represented by a simple power law. It is expressed by the equation that relates flow stress to the plastic strain:

$$\sigma = K(\varepsilon_p)^n$$

where K is the monotonic strength coefficient (intercept at plastic strain $\varepsilon_p = 1$) and n is the work-hardening or strain-hardening exponent. An increase in particulate reinforcement content in the 2014 metal matrix is observed to have no influence on the monotonic strain hardening or work hardening exponent (n) of the 2014/Al_2O_3 MMCs. While an increase in test temperature from 100 to 180 °C degraded both stiffness (elastic modulus) and strength (yield strength and ultimate tensile strength) of the 2014/Al_2O_3/xxp MMCs, it was found to have little to no influence on work hardening or strain hardening. However, consistent with the degradation in strength, the monotonic strength coefficient for both the 2014/Al_2O_3/10p and 2014/Al_2O_3/15p composites decreased at the higher test temperature, that is, with an increase in test temperature from 100 to 180 °C. The monotonic stress–strain curves for the two MMCs, at the two test temperatures, are compared in Fig. 8.

Several mechanisms of strengthening or hardening have been proposed which, either independently or in synergism, are considered responsible for the improved strength of discontinuously-reinforced metal matrices. The plausible mechanisms for discontinuous particulate-reinforced aluminium alloy metal matrix composites include:

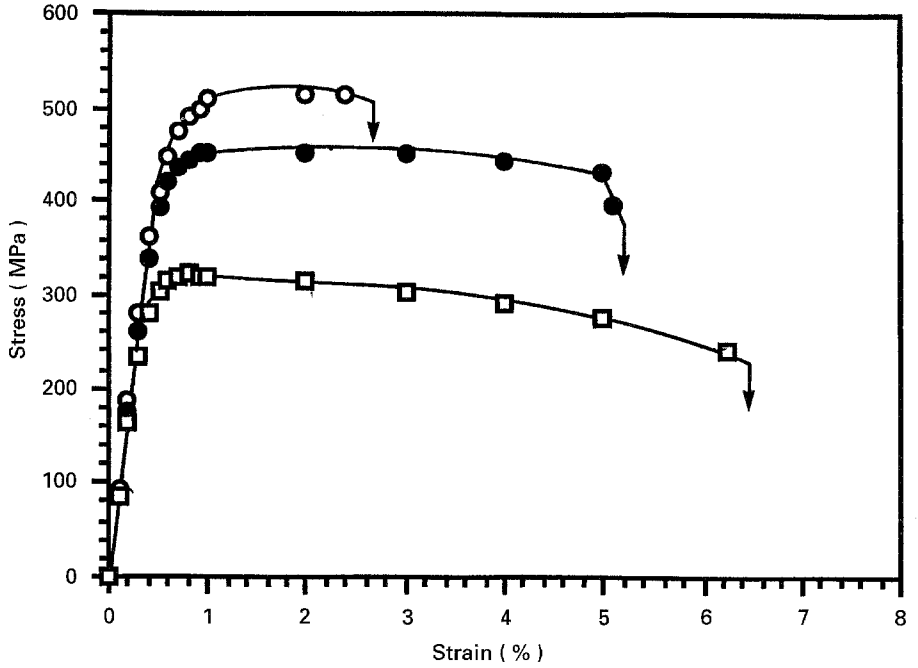

Figure 6 Effect of test temperature on engineering stress engineering strain curves of the $2014/Al_2O_3/15p$ composite. Key: (○) 25 °C; (●) 100 °C; (□) 180 °C.

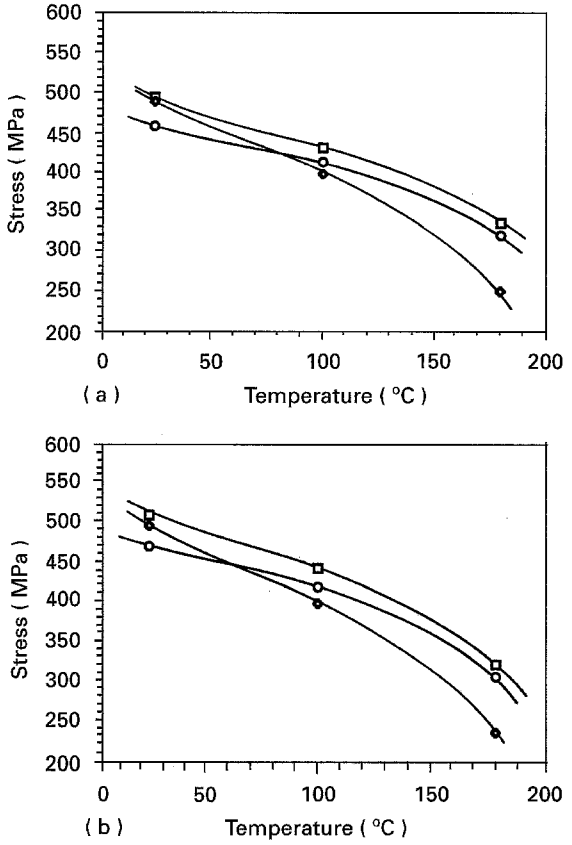

Figure 7 Variation of strength with test temperature: (a) $2014/Al_2O_3/10p$ composite; and (b) $2014/Al_2O_3/15p$ composite. Key: (○) yield; (□) ultimate; (◇) Fracture.

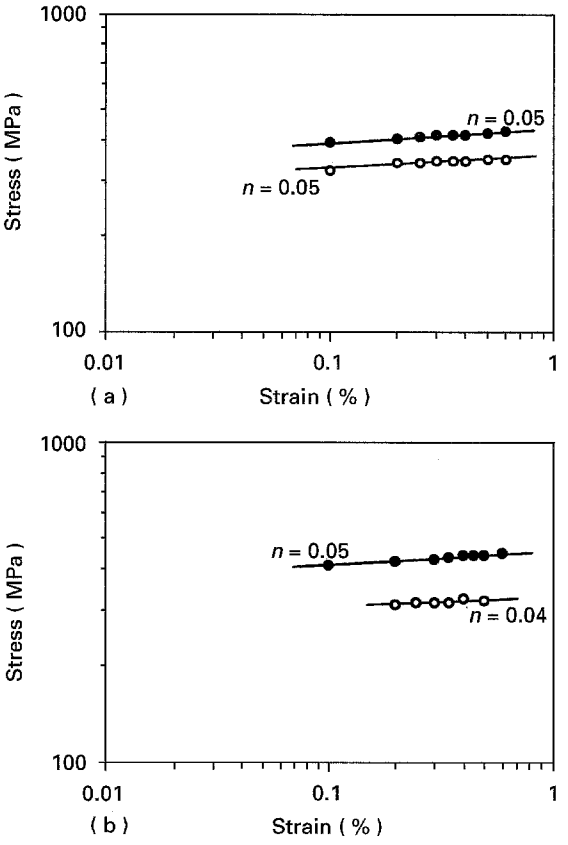

Figure 8 Influence of test temperature on monotonic stress-strain response of the composites: (a) $2014/Al_2O_3/10p$ composite, and (b) $2014/Al_2O_3/15p$ composite. Key: (○) 180 °C; (●) 100 °C.

1. An overall strengthening resulting from strength of the individual constituents of the composite, as per the classical rule-of-mixtures (ROM) theory [26].

2. Classical composite strengthening through load transfer between the ductile aluminium alloy matrix and the hard and brittle ceramic particle reinforcement [27–29]. Load transfer is largely dependent on bond integrity at the particulate–matrix interfaces.

3. Enhanced dislocation density in the aluminium alloy matrix due to the presence of the hard, brittle

and discontinuous particulate reinforcement phase [30–33]. The generation of dislocations arises from intrinsic differences in coefficients of thermal expansion (CTE) between the continuous metal matrix and the discontinuous particulate reinforcement phase [34, 35]. When the composite is cooled from the elevated temperatures of annealing and/or processing, misfit strains result due to differences in thermal contraction at the matrix–particle interface. The resultant misfit stresses are:

(a) relieved by the generation of dislocations through the "punch-out" mechanism to accommodate both the misfit strain and shape change the matrix cannot make due to the presence of the hard particulate reinforcement phase, and/or
(b) stored as thermal residual stresses.

Continuum-based and dislocation-based models have shown that the misfit strains are highly localized, with concomitant high residual stresses and/or high density of dislocations adjacent to the particulate reinforcements. The higher dislocation density tends to locally work harden the matrix and thus modify plastic response. The dislocation density can be estimated from the equation:

$$\varepsilon_p = \rho L \mathbf{b}$$

where ε_p is the plastic strain, ρ is the dislocation density (m^{-2}) generated, L is the distance moved by the generated dislocation, and **b** the Burgers vector of aluminium. The magnitude of dislocation density increase is related to both the volume fraction of reinforcement particles (V_f) and their size. Smaller-sized particles will increase the average dislocation density and thus the resultant residual stresses. The residual stresses are large enough to promote plastic deformation, i.e. the generation of dislocations. These dislocations can be defined as slip dislocations.

4. By the inhibition of plastic relaxation at the matrix–particle interfaces. Plastic relaxation is a mechanism by which local stress concentration due to accumulating dislocations is relieved and the mechanism also results in the generation of secondary dislocations at the interface [36, 37]. The ease and extent of plastic relaxation is governed by competing and mutually interactive influences of dislocation density, volume fraction of the discontinuous particulate reinforcements and matrix strengthening precipitates and particles. When plastic relaxation is restrained, void formation is favoured to occur due to dislocation build-up at the reinforcing particles.

5. The presence of an increased dislocation density favours formation of smaller subgrain size in the discontinuously-reinforced metal matrix resulting in subgrain strengthening being a significant contributing factor to the strength of the composite [30, 38, 39]. A small subgrain size results from a high density of dislocations generated by the thermal stress mismatch. The most appealing rationale for the formation of subgrain boundaries is that it presents an ideal lower-energy dislocation configuration [39].

6. Residual stresses generated in the composite matrix and plastic strains achieved adjacent to the particulate reinforcements due to competing and mutually interactive influences of: (a) mismatch (6 : 1) in coefficients of thermal expansion between components of the composite; the matrix and the reinforcement [40–42], and (b) during far-field tensile loading [43]. The residual stress induced in an aluminium alloy matrix will be tensile in nature [44–46]. The magnitude of this stress depends on:

(i) volume fraction, morphology and size of the discontinuous reinforcement phase, and
(ii) effective temperature change during heat treatment.

In the case of particulate reinforcements, in the form of spheres, the average residual stress in the matrix will be pure hydrostatic tension which has little to no influence on long-range dislocation motion. The average residual stress decreases as the size of the reinforcement phase increases. Since the residual stress is in tension, it is a negative contribution to the overall strengthening of the aluminium alloy-based MMC.

7. Strengthening arising from constrained plastic flow and triaxiality in the ductile matrix due to the presence of discontinuous particulate reinforcements [39, 47, 48]. As a result of the elastically deforming particulates resisting plastic flow of the ductile metal matrix, an average internal stress or back stress $\{\sigma_b\}$ is developed.

8. Contributions arising from competing influences of back stress in the plastically deforming composite matrix [49] and due to plastic relaxation by the formation of prismatic dislocation loops around the hard and brittle reinforcing particles [33, 41].

9. Intrinsic differences in texture between the aluminium alloy composite matrix and the unreinforced matrix material [39].

In this 2014/Al_2O_3/xxp MMC, with large CTE mismatch strain, the plastic deformation of the soft and ductile 2014 matrix, in the presence of the hard and brittle discontinuous Al_2O_3 particulate reinforcements, is non-uniform primarily due to the elastic particles resisting plastic flow of the metal matrix. The plastic deformation induced dislocations or slip dislocations become dominant when the plastic strain exceeds the thermal mismatch strain, at which point the two effects act in synergism so that they can be lumped together. The increased strength of this Al_2O_3 particulate-reinforced 2014 aluminium alloy MMC, due to dislocation generation, can be estimated using the relationship:

$$\Delta\sigma_y = \alpha G \mathbf{b} \rho^{0.5}$$

where $\Delta\sigma_y$ is the increase in yield strength of the composite over that of the unreinforced matrix material, G is the shear modulus (GPa) of the matrix metal, **b** is the Burgers vector, ρ is the average increase in dislocation density of the composite matrix over that of the matrix density, and α is a geometric constant and equal to 1.25 for aluminium [50]. The dislocation generation due to CTE mismatch, in a two-phase material, has been confirmed by other investigators [33, 39, 51]. Taya and Mori [52] and subsequently Mochida *et al.* [46] have shown that the punching of

dislocations generated by CTE mismatch strain in a particulate-reinforced metal matrix is sufficiently extensive to cover most of the matrix domain. The dislocations generated by CTE mismatch strain can at best be considered as an example of "geometrically necessary" dislocations defined by Ashby [53]. The "geometrically necessary" dislocations occur in order to permit compatible deformation in a system having geometrical constraints such as hard Al_2O_3 particles which deform elastically while the surrounding 2014 aluminium alloy metal matrix is ductile and undergoes plastic deformation. The "geometrically necessary" dislocations become essential when deformation occurs without the formation of voids around the hard and elastically deforming particles.

The primary factor contributing to the increase in flow stress of the discontinuous Al_2O_3 particulate-reinforced 2014 matrix over the unreinforced matrix alloy is due to the thermal residual stresses. The thermal stress is proportional to the CTE mismatch strain if the dislocations generated by CTE mismatch strain is dominant. The mismatch strain ε_α induced in the reinforcing particulate is:

$$\varepsilon_\alpha = (\alpha_p - \alpha_M)\,\Delta T$$

where

(i) α_p and α_M are coefficients of thermal expansion (CTE) of the reinforcing particle and the aluminium alloy metal matrix, respectively, and both the matrix and the reinforcing particle are assumed to be isotropic in stiffness and CTE.

(ii) ΔT is the net temperature $(T_o - T_{ambient})$ change when the particulate-reinforced metal matrix is quenched from an elevated temperature.

Based on the results obtained in this study and an examination of all of the plausible strengthening mechanisms, the contributions to strengthening of this Al_2O_3 particle-reinforced 2014 metal matrix arises from the concurrent and mutually interactive influences of the following three mechanisms:

(a) Strengthening due to large differences in coefficients of thermal expansion between constituents of the composite, aluminium alloy and the Al_2O_3 particulate reinforcements, resulting in misfit strains due to differential thermal contraction at the matrix–particle interfaces. The misfit strain and resultant misfit stress generates dislocations. The increased dislocation density generated to accommodate the misfit strain provides a significant contribution to strengthening of the metal matrix.

(b) The dislocations which are introduced during processing are not completely annihilated by the annealing treatment. Consequently, they become trapped at the Al_2O_3 particles resulting in local regions of high dislocation density, that is, the density is highest near the reinforcement particle and tends to decrease at regions away from the particle. A high dislocation density results in a small subgrain size with concomitant contribution to strength of the composite matrix.

(c) Strengthening arising from constrained plastic flow and triaxiality in the ductile metal matrix due to the presence of discontinuous particulate reinforcements [39, 48, 49]. As a result of the elastically deforming particles resisting plastic flow of the metal matrix, an average internal stress or back stress $\{\sigma_b\}$ is generated.

4.3. Tensile fracture behaviour

The tensile fracture surfaces are helpful in elucidating microstructural effects on the ductility and fracture properties of the $2014/Al_2O_3/xxp$ composites. It is fairly well established that the fracture of unreinforced alloys is associated with the events of void nucleation and growth, with the nucleation occurring at coarse constituent particles present in the microstructure [54, 55]. An essential requirement for void nucleation is the development of a critical normal stress across the particle or at the particle–matrix interfaces [56]. In the unreinforced metal matrix the nucleation of cavities and voids occurs by the concurrent and mutually competitive influences of:

(a) cracking of the hard and brittle inclusions that deform elastically, and

(b) decohesion at the interfaces between the elastically deforming particle and the plastically deforming metal matrix.

At room temperature (27 °C) the $2014/Al_2O_3/xxp$ composites exhibited limited ductility, on a macroscopic scale, with fracture essentially normal to the tensile stress axis. However, high magnification examination of the tensile fracture surface revealed features reminiscent of both ductile and brittle mechanisms. Representative fractographs of the tensile fracture surface of the $2014/Al_2O_3/10p$ and $2014/Al_2O_3/15p$ composites are shown in Figs 9–14.

4.3.1. Composite $2014/Al_2O_3/10p$

On a macroscopic scale, fracture surfaces of this composite were essentially flat and normal to the tensile stress axis at both room temperature (27 °C) and the elevated temperature (180 °C). However, the surfaces were relatively rough when viewed on a microscopic scale (Fig. 9a). At ambient temperature (27 °C) the fractured surfaces revealed the Al_2O_3 particles surrounded by ductile regions described as tear ridges (Fig. 9b), particle cracking (Fig. 9c) and decohesion at the matrix–particle interfaces (Fig. 9d). No major difference in tensile fracture features was evident at the higher test temperature (180 °C). The matrix of this composite was covered with microvoids of varying size (Fig. 10a). The voids were intermingled with tear ridges and isolated regions of dimpled rupture (Fig. 10b). The submicrometre-sized dimples are indicative of the improved ductility at this temperature.

4.3.2. Composite: $2014/Al_2O_3/15p$

At both 27 °C (Fig. 11) and 180 °C (Fig. 12) tensile fracture surfaces of this composite were flat and normal to the stress axis when viewed on a macroscopic scale but rough when viewed on a microscopic scale

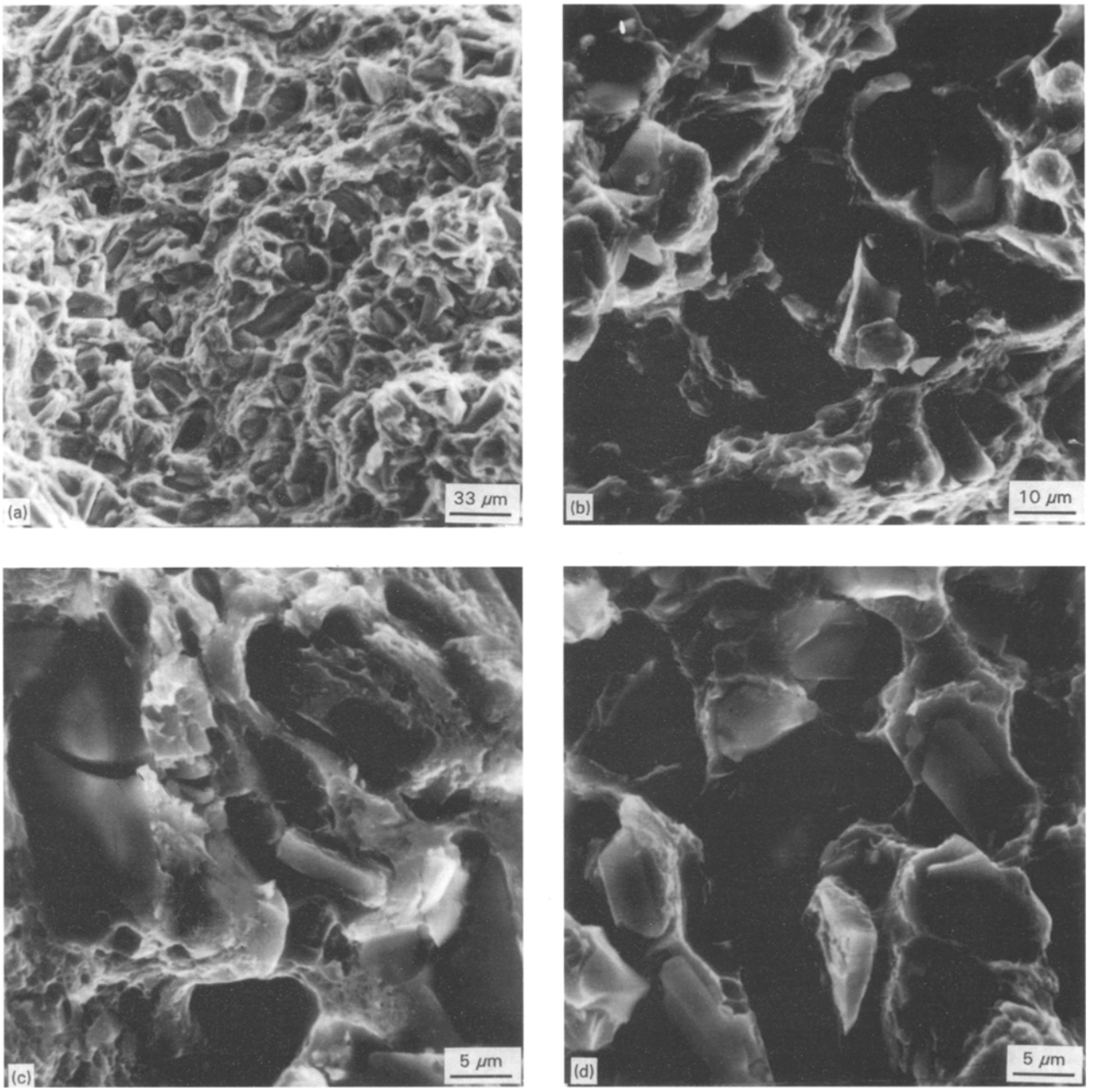

Figure 9 Scanning electron micrograph of the tensile fracture surface of the 2014/Al_2O_3/10p composite deformed at 27 °C.

(Fig. 11a). The matrix of this composite revealed combinations of tear ridges (Fig. 11b), cracking of the particles and decohesion at the interfaces (Fig. 11c). Following an early initiation of damage, subsequent accumulation, growth and linkage in the matrix resulted in brittle failure. At the higher test temperature (180 °C) the degree of particle cracking (Fig. 12b) and decohesion at particle–matrix interfaces increased (Fig. 12c). The matrix of the composite was covered with isolated microvoids of varying size (Fig. 11a). Two distinct types of dimples were observed, one surrounding the Al_2O_3 particles (Fig. 12d) and the other, smaller and shallower, with the matrix phases and inclusions. Multiple microcracks were observed in regions of particulate agglomeration, which contributed to the observed degradation of ductility.

The constraints in deformation caused by the presence of the hard and brittle Al_2O_3 particles in the soft and ductile aluminium alloy matrix and the resultant development of a triaxial stress state, in the soft and ductile metal matrix, aids in limiting flow stress of the composite matrix and favours:

(a) void initiation and growth in the matrix, and
(b) debonding at the particle–matrix interfaces.

Furthermore, as a consequence of the deformation constraints induced by the hard and brittle Al_2O_3 particulate reinforcements, a higher applied stress is required to initiate plastic deformation in the matrix. This translates to a higher elastic constant and higher yield strength of the composite. Under the influence of a far-field tensile load the voids appeared to have undergone limited growth confirming a possible contribution from particle constraint-induced triaxiality on failure of the composite matrix. Particle failure is governed by competing influences of local plastic constraints, particle size and agglomeration. The local plastic constraints are particularly important for the

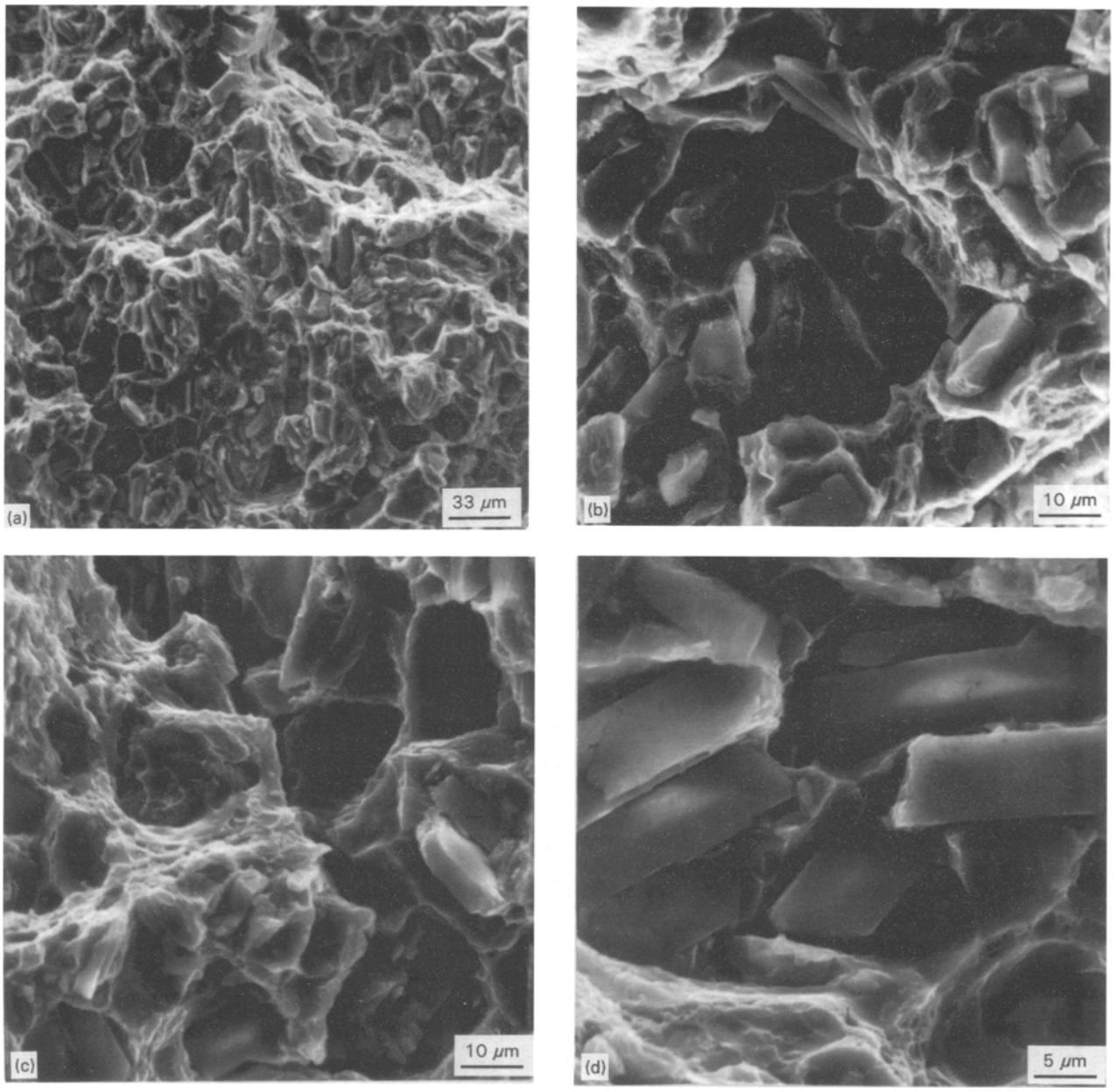

Figure 10 Scanning electron micrograph of the tensile fracture surface of the 2014/Al_2O_3/10p composite deformed at 180 °C.

larger-sized particles and for particle clusters during composite fracture [43]. Examination of the fracture surfaces revealed damage to be highly localized at the Al_2O_3 reinforcing phase through cracked particles and interfacial failure or decohesion with little evidence of void formation away from the cracked or fractured particle. This suggests that the plastic strain becomes localized during the early stages of tensile deformation. The intrinsic brittleness of the reinforcing particles (Al_2O_3) coupled with the propensity for it to fracture due to localized deformation results in particle cracking and particle–matrix interface debonding (Fig. 13) being the dominant damage mode. The higher yield strength coupled with damage to the composite microstructure from the conjoint influence of particle cracking and decohesion at the interfaces results in a decrease in strain-to-failure or inferior ductility of the 2014/Al_2O_3/xxp MMC. Furthermore, neglecting any contribution from the matrix–particle interfaces, the triaxial stresses generated during far-field tensile loading favours limited growth of the microvoids in the matrix of the composite. The limited growth of the voids during far-field tensile loading coupled with lack of their coalescence as a dominant fracture mode for the 2014/Al_2O_3/xxp MMCs clearly indicates that the deformation properties of the 2014 matrix are significantly altered by the presence of the discontinuous Al_2O_3 particulate reinforcements. The presence of Al_2O_3 particulates raises the hydrostatic component of stress and, hence, their distribution is an important factor governing fracture of the composite [32]. In particulate-rich regions of the matrix, fracture occurs early and the damage propagates rapidly among the reinforcing particle agglomerate. However, the reinforcement-lean regions, i.e. the metal matrix, aids in retarding the progression and linkage of the damage.

Fracture of the brittle Al_2O_3 particles coupled with concurrent failure of the surrounding matrix results in the formation of fine voids at the particle–matrix

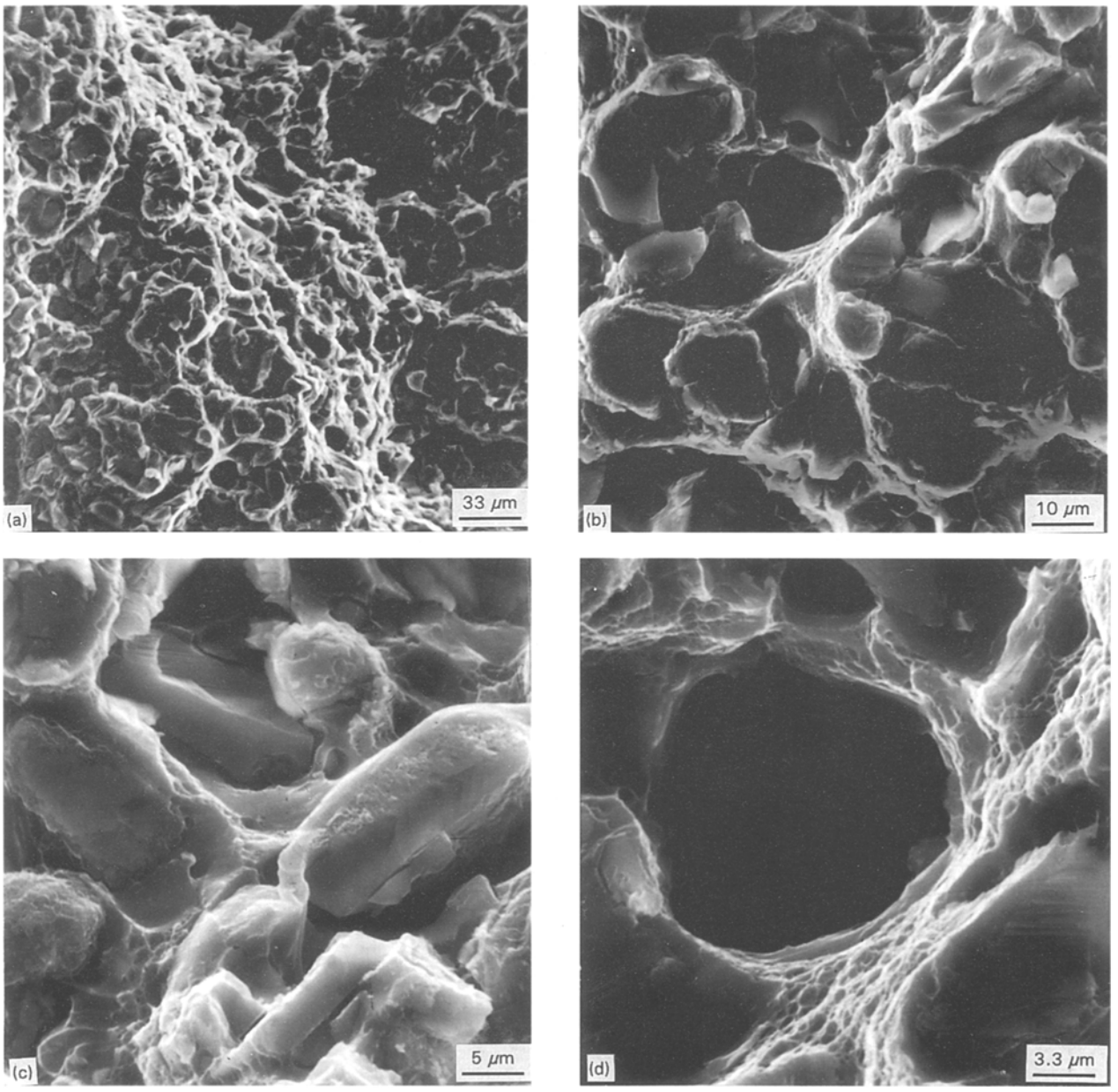

Figure 11 Scanning electron micrograph of the tensile fracture surface of the 2014/Al_2O_3/15p composite deformed at 27 °C.

interfaces. Very few of the fine microvoids coalesce and the halves of these voids are the shallow dimples observed surrounding the cracked particles. The lack of formation of ductile dimples in the matrix, as a dominant fracture mode, is attributed primarily to the constraints on plastic flow caused by the presence of the discontinuous Al_2O_3 particles, i.e. the deformation incompatibility between the plastically deforming metal matrix and the elastically deforming Al_2O_3 reinforcement phase, and not due to limited ductility of the 2014 aluminium alloy metal matrix. The constraints imposed on plastic flow favours the formation of tear ridges at and between the reinforcing particulates. With an increase in reinforcement content, fracture was found to be dominated by cracking of the Al_2O_3 particles on account of their intrinsic brittleness (Fig. 12b). With a progressive increase in strain, the larger-sized particles fracture first, at low values of applied strain, followed by the smaller-sized particles. Based on an observation of the tensile fracture surfaces, it is seen that the fracture plane of cracked particles is perpendicular to the loading axis, suggesting the importance of the tensile stress in inducing particle fracture (Fig. 13a). The early cracking of reinforcing Al_2O_3 particles coupled with rapid damage propagation in the particle-rich regions are the two contributing factors responsible for the lower tensile ductility of the 2014/Al_2O_3/xxp composites.

The overall "damage" resulting from uniaxial straining of the 2014/Al_2O_3/xxp MMC arises from the conjoint action of:

(a) Damage associated with the discontinuous Al_2O_3 reinforcement such as particle cracking and decohesion at the particle–matrix interfaces.

(b) Lattice damage such as dislocations and point defects, coupled with residual stress effects associated with the presence of Al_2O_3 particles [43].

For the Al_2O_3 particulates, dispersed in the 2014 matrix, to completely fracture they must be loaded to

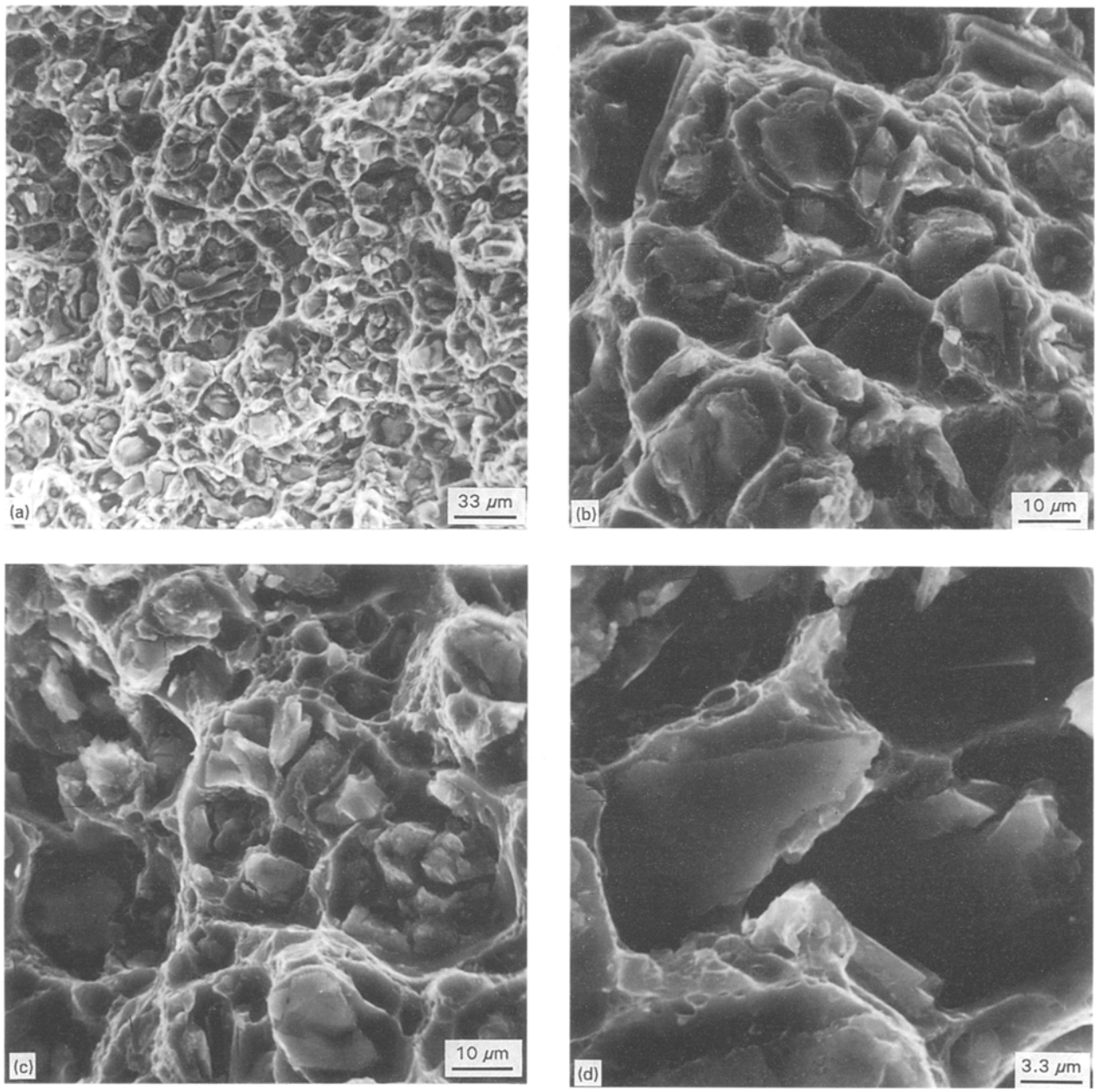

Figure 12 Scanning electron micrograph of the tensile fracture surface of the 2014/Al_2O_3/15p composite deformed at 180 °C.

their fracture stress. This is achieved globally by the tensile stress and locally by shear loading through the interface. The extent of particle loading by the shear mechanism is dependent on the aspect ratio of the reinforcing Al_2O_3 particles. For the case of symmetrically packed particles in the metal matrix, the aspect ratio (S_s) for maximum loading is [43]:

$$S_s = \sigma_{Al_2O_3} / \tau_i$$

where $\sigma_{Al_2O_3}$ is the strength of the particle and τ_i is the interfacial shear strength. The shear mechanism ignores any end loading effects which would tend to exert additional stress on the particle. A careful observation of the tensile fracture surface of the two composites revealed in excess of 50 per cent of the reinforcing Al_2O_3 particles had fractured during tensile deformation. This indicates that not all of the particles were loaded to their fracture stress suggesting the non-uniform distribution of the particles in the metal–matrix. This situation is further complicated by:

1. The mismatch strain and concomitant internal stress in the composite matrix due to differences in the thermal expansion coefficient (6 : 1) between the Al_2O_3 particles and the matrix. Assuming near spherical shape particles, the mismatch strain (ε_α) that will be induced in the particles will be given by Equation 4. For the Al_2O_3 particles fracture to occur, the applied far-field tensile stress will have to first overcome any internal stress present in the particle.
2. Loading the particles through the misfit strain generated during plastic flow as a result of the difference in elastic modulus between the hard and brittle Al_2O_3 particle and the soft and ductile 2014 matrix.

For this particulate-reinforced 2014 metal matrix the majority of damage is associated with particulate clusters, and is in the form of cracked particles and

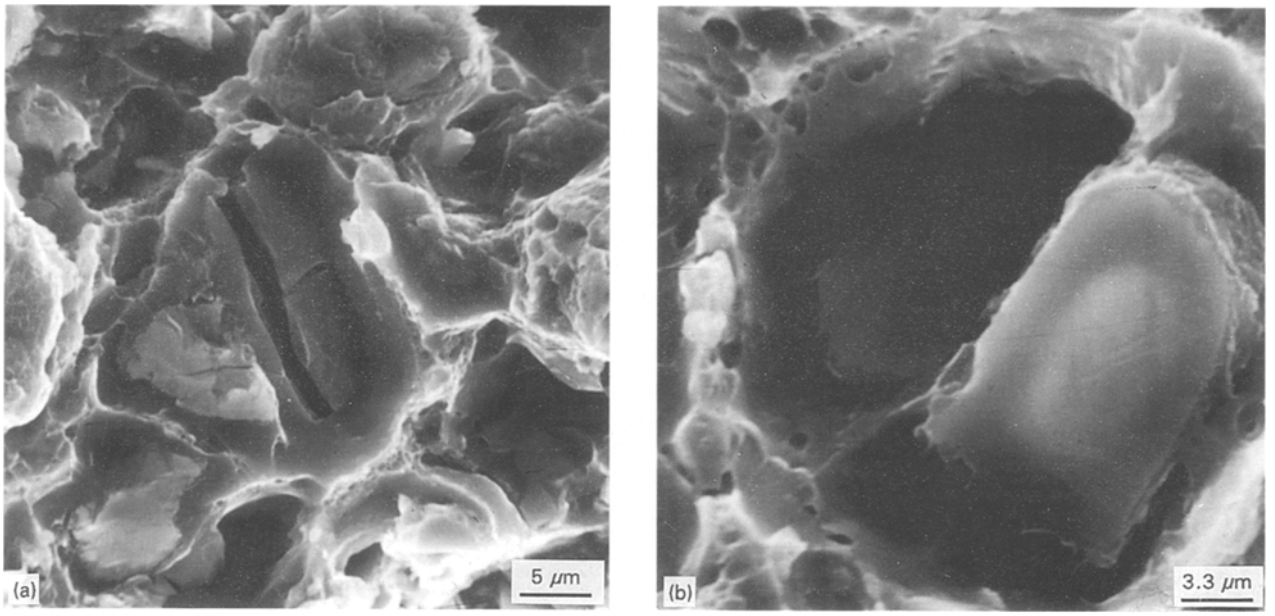

Figure 13 Scanning electron micrographs showing cracked particles and debonding at matrix–particle interface.

voids which have formed around the particles (Figs 11d and 12b). The fracture initiates by particle cracking coupled with decohesion of the matrix surrounding and between the particulate reinforcements. Final fracture is achieved by damage propagation through the matrix between particle-rich regions. Few of the voids generated by particle cracking did not grow extensively in the tensile stress direction, which is generally the case in ductile fracture of unreinforced aluminium alloys. The lack of extensive void growth in this Al_2O_3 particulate-reinforced 2014 aluminium alloy metal matrix also suggests that the fracture strain is critically controlled by both the void nucleation strain and associated linkage strain.

5. Conclusions

Based on the results of this investigation on the influence of volume fraction of particulate reinforcement and test temperature on tensile deformation and fracture behaviour of 2014 aluminium alloy discontinuously-reinforced with Al_2O_3 particulates, the following are the key observations:

1. The microstructure of the as-received 2014/Al_2O_3 composites revealed a non-uniform dispersion of the Al_2O_3 particles along the three orthogonal directions of the extruded plate. At regular intervals, an agglomeration of the Al_2O_3 particles, of varying size, was observed.

2. Increase in the amount of discontinuous Al_2O_3 particulate reinforcement in the 2014 aluminium alloy metal matrix increased the elastic modulus at ambient temperature and elevated temperature of 100 °C. However, at the elevated temperature of 180 °C the elastic modulus decreased with increased particulate reinforcement in the 2014 metal matrix.

3. The increased strength of this 2014/Al_2O_3 composite is rationalized in terms of mutually competitive influences of mechanisms based on: (a) an increase in dislocation density in the matrix due to the presence of Al_2O_3 particulate reinforcements, (b) residual stresses generated in the matrix due to intrinsic differences in thermal expansion coefficients between the composite constituents, and (c) strengthening from constrained plastic flow and triaxiality due to the presence of discontinuous particulate reinforcements.

4. The non-uniform size and dispersion of the Al_2O_3 particulates caused the particles to crack at low values of applied stress. The cracks initiated both at and near particle–matrix interfaces in regions of particle agglomeration. The tensile fracture surface revealed limited ductility or brittle appearance on a macroscopic scale, but at the microscopic level features reminiscent of locally ductile and brittle rupture mechanisms. The fracture surface revealed combinations of tear ridges, cracked particles and decohesion at interfaces.

5. Fracture of the particles coupled with failure of the matrix between particle clusters and decohesion of the matrix surrounding particles permits the microcracks to grow rapidly and link by fracture through the matrix resulting in macroscopically brittle appearance and resultant low ductility of the composite.

Acknowledgements

This research was supported by the Ohio Aerospace Institute (Contract No.: OAI: CCRP-92-1-011) and Rockwell International Corporation, Rocketdyne Division (Program Manager: Mr K. Janowski). Sincere thanks and appreciation are extended to DURALCAN USA (Program Manager: Mr Charles Lane) for providing the material used in this study.

References

1. L. N. MUELLER, J. L. PROHASKA and J. W. DAVIS, in Proceedings of AIAA Aerospace Engineering Conference (AIAA, Los Angeles, California).

2. D. A. KOSS and S. M. COPLEY: *Metall. Trans.* **2A** (1971) 1557.
3. A. P. DIVECHA, C. R. CROWE and S. G. FISHMAN, "Failure Modes in Composites IV" (Metallurgical Society of American Institute of Mining, Metallurgical and Petroleum Engineers, Warrendale, PA, 1977) pp. 406–411.
4. A. P. DIVECHA, S. G. FISHMAN and S. D. KARMARKAR, *J. Met.* **33** (1981) 12.
5. M. TAYA and R. J. ARSENAULT, in "Metal Matrix Composites: Thermomechanical Behavior", (Pergamon Press, Elmsford, New York, 1989).
6. T. S. SRIVATSAN and T. S. SUDARSHAN: in "Rapid Solidification Technology: An Engineering Guide", edited by T. S. Srivatsan and T. S. Sudarshan (Technomic Publishing Inc., PA, 1993) pp. 603–700.
7. L. M. BROWN and W. M. STOBBS, *Phil. Mag.* **23** (1971) 1185.
8. S. V. NAIR, J. K. TIEN and R. C. BATES, *Int. Met. Rev.* **30** (1985) 285.
9. D. L. McDANELS, *Metall. Trans.* **16A** (1985) 1105.
10. S. DERMARKAR, *Met. Mater.* **2** (1986) 144.
11. W. H. HUNT, Jr, C. R. COOK and R. R. SAWTELL "Cost Effective High Performance Powder Metallurgy Aluminum Matrix Composites for Automotive Applications," SAE Technical Paper Series 910834, February 1991, Warrendale, PA.
12. W. R. EAST, *Mater. Eng.* March (1988) 33.
13. R. DeMEIS, *Aerosp. Amer.* March (1989) 26.
14. T. C. WILLIS, *Met. Mater.* August (1988) 485.
15. Y. SUGIMURA and S. SURESH, *Metall. Trans.* **23A** (1992) 2231.
16. P. K. LIAW and W. A. LOGSDON, *Eng. Fract. Mech.* **24** (1986) 737.
17. J. J. LEWANDOWSKI, C. LIU and W. H. HUNT, Jr, in "Interfacial Phenomenon in Composites: Processing, Characteristics and Mechanical Properties" (Metallurgical Society of American Institute of Mining, Metallurgical and Petroleum Engineers, Warrendale, PA, 1988).
18. J. K. SHANG and R. O. RITCHIE, *Metall. Trans.* **20A** (1989) 897.
19. *Idem, Acta Metall.* **37** (1989) 2267.
20. J. J. LEWANDOWSKI, C. LIU and W. H. HUNT, Jr. *Mater. Sci. Eng.* **107A** (1989) 49.
21. D. L. DAVIDSON, *J. Mater. Sci.* **24** (1989) 681.
22. *Idem, Eng. Fract. Mech.* **33** (1989) 965.
23. M. MANOHARAN and J. J. LEWANDOWSKI, *Acta Metall.* **38** (1990) 489.
24. *Idem, Scripta Metall.* **23** (1989) 301.
25. T. S. SRIVATSAN and J. MATTINGLY, *J. Mater. Sci.* **23** (1993) 611.
26. G. J. DVORAK, in "Metal Matrix Composites: Mechanisms and Properties", edited by R. K. Everett and R. J. Arsenault (Academic Press, San Diego, CA, 1991) pp. 1–70.
27. V. C. NARDONE, *Scripta Metall.* **21** (1987) 1313.
28. R. L. MEHAN, "Metal Matrix Composites", ASTM STP (American Society for Testing and Materials, Philadelphia, 1968) p. 43.
29. G. J. DVORAK, M. S. M. RAO and J. Q. TARN, *J. Compos. Mater.* **7** (1973) 194.
30. R. J. ARSENAULT and R. M. FISHER, *Scripta Metall.* **17** (1983) 67.
31. R. J. ARSENAULT, *Mater. Sci. Eng.* **64** (1984) 171.
32. R. J. ARSENAULT, L. WANG and C. R. FENG, *Acta Metall. Mater.* **39** (1991) 47.
33. M. VOGELSANG, R. J. ARSENAULT and R. M. FISHER, *Metall. Trans.* **127A** (1986) 379.
34. Y. FLOM and R. J. ARSENAULT, *Mater. Sci. Eng.* **77** (1986) 191.
35. M. F. ASHBY and L. JOHNSON, *Phil. Mag.* **20** (1969) 1009.
36. F. J. HUMPHREYS, in 9th Riso International Symposium on Metallurgy and Materials Science, Mechanical Properties and Physical Behavior of Metals and Composites, Roskilde, Denmark, 1988, p. 51.
37. A. S. ARGON, J. IM and R. SAFOGLU, *Metall. Trans.* **6A** (1975) 825.
38. R. J. ARSENAULT, in "Composite Structures", edited by I. H. Marshall (Elsevier Science Publishers, London, 1987) pp. 70–90.
39. *Idem*, in "Metal Matrix Composites: Mechanisms and Properties, edited by R. K. Everett and R. J. Arsenault (Academic Press, San Diego, 1991) pp. 79–87.
40. W. J. CLEGG, *Acta Metall.* **36** (1988) 2141.
41. M. TAYA, K. E. LULAY and D. J. LLOYD: Acta Metallurgica Materialia, Vol. 39, 1991, pp. 73–80.
42. M. TAYA, *Mater. Trans.: Jpn Inst. Met.* **32** (1991) 1.
43. D. J. LLOYD, *Acta Metall.* **39** (1991) 59.
44. R. J. ARSENAULT, *J. Compos. Techn. Res.* **10** (1988) 140.
45. R. J. ARSENAULT and M. TAYA, *Acta Metall.* **35** (1987) 651.
46. T. MOCHIDA, M. TAYA and D. J. LLOYD, *Mater. Trans. JIM.* **32** (1991) 931.
47. D. C. DRUCKER, in "High Strength Materials", edited: V. F. Zackey (Wiley Interscience, New York, 1965).
48. T. W. BUTLER and D. C. DRUCKER, *J. Appl. Mech.* **40** (1973) 780.
49. K. TANAKA and T. MORI, *Acta Metall.* **18** (1979) 931.
50. N. HANSEN, *Acta Metall.* **25** (1977) 863.
51. K. K. CHAWLA and M. METZGER, *J. Mater. Sci.* **17** (1972) 34.
52. M. TAYA and T. MORI, *Acta Metall.* **35** (1987) 155.
53. M. F. ASHBY, *Phil. Mag.* **21** (1970) 399.
54. F. A. McCLINTOCK, "Ductility" (American Society for Metals, Metal Park, Ohio, 1968) pp. 256–261.
55. R. H. VANSTONE, T. B. COX, J. R. LOW, Jr and J. A. PSIODA, *Int. Met. Rev.* **30** (1975) 157.
56. A. S. ARGON, J. IM and R. SAFOGLU, *Metall. Trans.* **6A** (1975) 825.

Received 7 March 1994
and accepted 16 August 1995